

# Just on Time: Token-Level Early Stopping for Diffusion Language Models

Zahar Kohut<sup>1,2\*</sup>

Severyn Shykula<sup>1,2\*</sup>

Taras Rumezhak<sup>1</sup>

Dmytro Khamula<sup>1,2</sup>

Volodymyr Karpiv<sup>1</sup>

Mykola Vysotskyi<sup>1,2</sup>

<sup>1</sup>SoftServe Inc.

<sup>2</sup>Ukrainian Catholic University

## Abstract

Diffusion language models generate text through iterative refinement, a process that is often computationally inefficient because many tokens reach stability long before the final denoising step. We introduce a training-free, token-level early stopping approach that identifies convergence independently at each position. Our method leverages lightweight signals derived from the model’s predictions and local context to dynamically determine when individual tokens can be finalized. This yields adaptive per-token freezing without task-specific fine-tuning, substantially reducing the total number of diffusion steps required. Across diverse benchmarks, spanning mathematical reasoning, general question answering, and scientific understanding, our approach achieves state-of-the-art efficiency gains while preserving generation quality.

## 1 Introduction

Autoregressive (AR) models dominate the current landscape of large language models, generating text through sequential left-to-right token prediction. While remarkably effective, this paradigm imposes inherent constraints: each token must wait for all preceding tokens, limiting parallelism and preventing the model from leveraging future context during generation.

Diffusion language models (DLMs) have emerged as a compelling alternative [2]. Rather than generating tokens sequentially, DLMs begin with a fully masked sequence and progressively refine it through iterative denoising, enabling parallel token prediction and bidirectional context integration. Recent work has demonstrated that DLMs can achieve competitive performance with strong autoregressive models on tasks ranging from in-context learning to instruction following [15, 24].

Despite this promise, *decoding efficiency* remains a challenge for DLMs. Generation proceeds through a reverse-diffusion chain requiring many refinement steps, and practitioners must choose step budgets conservatively to avoid quality degradation. This leads to unnecessary computation: many tokens converge to stable predictions well before the final denoising step [11], yet standard decoding continues refining them regardless.

We introduce **JOT** (**Just on Time**), a training-free method for per-token early stopping in diffusion language models. Rather than applying a global stopping criterion, JOT monitors prediction confidence at each position independently and finalizes tokens as soon as they exceed a threshold. This allows different positions to exit at different steps, concentrating computation on tokens that genuinely require further refinement.

We evaluate JOT on Dream-7B-Instruct and LLaDA-8B-Instruct across four benchmarks: GSM8K, MMLU, HellaSwag, and HumanEval. Our experiments demonstrate that JOT achieves favorable speed-quality trade-offs, providing up to 5.5 $\times$  speedup on GSM8K and 19.6 $\times$  on HumanEval while maintaining score within 3 per cent of full decoding. Ablation studies confirm that both threshold selection and spatial modulation contribute to performance.

**Contributions.** We summarize our main contributions as follows:

- We propose JOT, a training-free, per-token early stopping method for diffusion language models that adapts acceptance thresholds based on spatial proximity to resolved context.

\*Equal contribution.

- We conduct comprehensive experiments on Dream-7B and LLaDA-8B across four benchmarks, analyzing speed-quality trade-offs against existing early-exit methods.
- We provide detailed ablation studies isolating the effects of threshold selection and spatial modulation, offering practical guidance for hyperparameter configuration.

## 2 Related Work

### 2.1 Diffusion Language Models

Diffusion models have achieved remarkable success in continuous domains such as image and audio generation [9, 20]. Extending this paradigm to discrete data like text presents unique challenges, as the standard Gaussian noise process does not directly apply to categorical variables. Two main approaches have emerged: embedding-based methods that project tokens into continuous space before applying standard diffusion [12, 7], and discrete diffusion methods that define corruption processes directly over the vocabulary.

D3PM [2] established a foundational framework for discrete diffusion by modeling the forward process as a discrete-state Markov chain with learnable transition matrices. This work demonstrated that diffusion principles could be adapted to categorical data while preserving the variational lower bound interpretation. Subsequent work on score entropy discrete diffusion (SEDD) [13] connected score-based perspectives with likelihood-based training for discrete sequences.

### 2.2 Masked Diffusion Language Models

Among discrete diffusion formulations, masked (absorbing-state) diffusion has emerged as particularly effective for language modeling. In this setup, the forward process progressively replaces tokens with a special mask token, and the reverse process learns to predict the original tokens from partially masked sequences.

MDLM [19] formalized this paradigm with a substitution-based reverse parameterization (SUBS) and derived a simplified, Rao-Blackwellized objective that reduces to a weighted mixture of classical masked language modeling losses. This connection to BERT-style training [5] enables leveraging established architectural choices while supporting principled generation via ancestral sampling.

LLaDA [15] scaled masked diffusion to 8B parameters, demonstrating that diffusion-based LMs can achieve competitive performance with autoregressive baselines across diverse tasks including in-context learning and instruction following. The model employs a standard pre-training and supervised fine-tuning pipeline, establishing that the core capabilities of large language models are not exclusive to autoregressive architectures.

Dream 7B [24] further advances the state of the art with practical training techniques including autoregressive model initialization and context-adaptive token-level noise rescheduling. The model demonstrates diffusion-specific advantages such as flexible generation order, infilling capabilities, and tunable quality-speed trade-offs.

### 2.3 Early Stopping for Diffusion Decoding

Recent work has observed that predictions often stabilize well before the final diffusion step, motivating early-exit strategies. Prophet [11] documents this “early answer convergence” phenomenon: on benchmarks such as GSM8K and MMLU, a large fraction of instances can be correctly decoded using only half of the prescribed steps. Prophet proposes a training-free early-commit rule that monitors the confidence gap between the top-2 predicted tokens and finalizes all remaining masked positions once this gap exceeds a threshold, achieving significant speedups with minimal quality degradation.

Complementary approaches focus on token-level stability signals. KLASS [10] introduces KL-Adaptive Stability Sampling, which uses the KL divergence between consecutive step distributions to identify stable predictions and unmask multiple tokens in parallel. SlowFast Sampling [22] alternates between exploratory and accelerated phases based on certainty and convergence criteria.

Orthogonal to reducing step counts, other efforts target per-step latency through caching mechanisms adapted to bidirectional attention [14, 21, 23].

## 3 Preliminaries

We introduce notation and background on discrete diffusion language models (DLMs).

### 3.1 Discrete Diffusion Language Models

Consider a vocabulary  $\mathcal{V}$  of size  $K$  augmented with a mask token  $[\text{M}]$ . A sequence of length  $L$  is denoted  $\mathbf{x} = (x^1, \dots, x^L)$  with  $x^i \in \mathcal{V}$ .

Autoregressive language models factorize the joint distribution as  $p(\mathbf{x}) = \prod_{i=1}^L p(x^i | x^{<i})$  and generate tokens sequentially from left to right. In contrast, discrete diffusion models define a generative process through the interplay of a forward corruption process and a learned reverse denoising process, enabling parallel refinement of all positions simultaneously.

**Forward process.** The forward process progressively corrupts a clean sequence  $\mathbf{x}_0$  by independently replacing tokens with the mask token. Let  $t \in [0, 1]$  denote the continuous noise level, where  $t = 0$  corresponds to clean data and  $t = 1$  to the fully masked state. The forward marginal factorizes over positions as  $q(\mathbf{x}_t | \mathbf{x}_0) = \prod_{i=1}^L q(x_t^i | x_0^i)$ , where

$$q(x_t^i | x_0^i) = \alpha_t \delta(x_t^i = x_0^i) + (1 - \alpha_t) \delta(x_t^i = [\text{M}]). \quad (1)$$

Here,  $\alpha_t \in [0, 1]$  is a monotonically decreasing noise schedule with  $\alpha_0 \approx 1$  and  $\alpha_1 \approx 0$ .

**Reverse process.** Generation proceeds by reversing the forward corruption: starting from a fully masked sequence  $\mathbf{x}_T$  at  $t = 1$ , the model iteratively predicts and unmasks tokens until reaching the clean state at  $t = 0$ . A neural network  $f_\theta$  parameterizes the reverse transition by producing a distribution over the vocabulary at each position:

$$p_\theta(\mathbf{x}_s | \mathbf{x}_t) = \prod_{i=1}^L p_\theta(x_s^i | \mathbf{x}_t), \quad 0 \leq s < t \leq 1. \quad (2)$$

For masked positions, the model predicts  $p_\theta(x_s^i | \mathbf{x}_t) = \text{Cat}(x_s^i; \pi_\theta^i(\mathbf{x}_t))$ , where  $\pi_\theta^i(\mathbf{x}_t) \in \Delta^K$  is the predicted distribution at position  $i$ . Unmasked tokens are preserved.

### 3.2 Iterative Sampling

Practical generation proceeds through  $T$  discrete steps. At step  $n$ , let  $\mathcal{M}_n = \{i : x_{t_n}^i = [\text{M}]\}$  denote the masked positions. The model computes predictions  $\pi_\theta^i(\mathbf{x}_{t_n})$  for all  $i \in \mathcal{M}_n$ , then selects a subset  $\mathcal{U}_n \subseteq \mathcal{M}_n$  to unmask based on a transfer schedule. A common strategy unmasks positions with the highest confidence  $\max_v \pi_\theta^i(\mathbf{x}_{t_n})_v$ , deferring uncertain positions to later steps.

### 3.3 Training Objective

DLMs minimize a variational upper bound on negative log-likelihood, which simplifies to a reweighted cross-entropy over masked positions:

$$\mathcal{L}(\theta) = -\mathbb{E}_{\mathbf{x}_0, t, \mathbf{x}_t} \left[ w(t) \sum_{i=1}^L \mathbf{1}[x_t^i = [\text{M}]] \log p_\theta(x_0^i | \mathbf{x}_t) \right], \quad (3)$$

where  $t \sim \mathcal{U}(0, 1)$  and  $w(t)$  is a time-dependent weight, commonly  $w(t) = 1/t$ .

## 4 Approach

We present **JOT (Just on Time)**, a training-free method for per-token early stopping in diffusion language models. The core idea is to finalize individual token predictions as soon as they exhibit sufficient confidence, rather than waiting for a fixed number of diffusion steps. Our approach adapts the acceptance threshold at each position based on spatial proximity to already-resolved tokens.

### 4.1 Overview

Standard DLM decoding runs for a predetermined number of steps  $T$ , unmasking tokens according to a transfer schedule. However, prior work has shown that predictions often stabilize well before the final diffusion step [11]. JOT exploits this observation by introducing an adaptive early-exit mechanism that operates at the token level: at each step, positions whose predictions exceed a dynamically computed confidence threshold are finalized immediately, removing them from further refinement.

The key components of our method are:

1. A *confidence metric* that quantifies prediction certainty at each masked position.
2. A *spatial modulation* that lowers the threshold for positions adjacent to already-unmasked tokens.

## 4.2 Confidence Metric

We measure prediction confidence using the ratio between the top two predicted probabilities. At each masked position  $i$ , the model produces logits  $\ell^i \in \mathbb{R}^K$ , which we convert to a probability distribution via softmax without temperature scaling:  $\pi_\theta^i(\mathbf{x}_t) = \text{softmax}(\ell^i) \in \Delta^K$ . By using unscaled logits, our confidence metric remains invariant to any temperature parameter applied during sampling, decoupling early-exit decisions from generation diversity settings. Denote the largest and second-largest probabilities as  $p_1^i$  and  $p_2^i$ , respectively. The confidence score is defined as:

$$r^i = \frac{p_1^i}{p_2^i + \epsilon}, \quad (4)$$

where  $\epsilon > 0$  is a small constant for numerical stability. This ratio captures how decisively the model favors its top prediction:  $r^i \approx 1$  indicates uncertainty between alternatives, while  $r^i \gg 1$  signals strong commitment to the leading candidate.

## 4.3 Spatial Modulation

Recent work on diffusion language model training has shown that positions with stronger local context—particularly those near already-decoded tokens—tend to experience lower noise level [24]. Dream’s CART weighting exploits this during training by applying context-adaptive noise rescheduling at the token level. We draw inspiration from this finding and apply analogous reasoning to inference: positions adjacent to already-unmasked tokens benefit from richer local context, making their predictions more reliable even at earlier steps. We capture this through a spatial softening factor based on proximity to resolved positions.

Let  $\mathcal{M}_n$  denote the set of masked positions at step  $n$ . The spatial weight at position  $i$  is computed using a geometric kernel over a window of radius  $D$ :

$$w^i = \sum_{\substack{j \notin \mathcal{M}_n \\ |i-j| \leq D}} \gamma^{|i-j|} \quad (5)$$

where  $\gamma \in (0, 1)$  is the decay rate controlling how quickly influence diminishes with distance. The spatial softening factor is the normalized weight:

$$\phi^i = \min \left( 1, \frac{w^i}{w_{\max}} \right), \quad (6)$$

where  $w_{\max} = 2 \sum_{d=1}^D \gamma^d$  is the maximum possible weight. Positions at the boundary of masked regions receive higher  $\phi^i$ , reflecting their enhanced contextual support.

## 4.4 Adaptive Threshold

The spatial softening factor modulates a position-specific acceptance threshold. The threshold at position  $i$  is interpolated between a maximum  $\tau_{\max}$  and minimum  $\tau_{\min}$ :

$$\tau^i = \tau_{\max} - (\tau_{\max} - \tau_{\min}) \cdot \phi^i. \quad (7)$$

Positions near unmasked tokens (high  $\phi^i$ ) receive lower thresholds, making them easier to finalize. Positions in the interior of masked regions retain the stricter threshold  $\tau_{\max}$ , requiring higher confidence before commitment.

## 4.5 Early-Exit Decision

At each step  $n$ , a masked position  $i \in \mathcal{M}_n$  is finalized if its confidence exceeds the adaptive threshold:

$$r^i \geq \tau^i. \quad (8)$$

When this condition is met, position  $i$  is assigned its top predicted token  $\hat{x}^i = \arg \max_v \pi_\theta^i(\mathbf{x}_{t_n})_v$  and removed from the set of masked positions. Positions that do not meet the threshold continue through the standard transfer schedule.

The complete procedure is summarized in Algorithm 1.

---

**Algorithm 1** JOT: Token-Level Early Stopping

---

**Input:** model  $f_\theta$ ; prompt  $\mathbf{x}_{\text{prompt}}$ ; generation length  $L$ ; steps  $T$   
**Parameters:**  $\tau_{\max}, \tau_{\min}, \gamma, D$   
Initialize  $\mathbf{x} \leftarrow [\mathbf{x}_{\text{prompt}}; \mathbf{M}] \times L$   
**for**  $n = 1$  **to**  $T$  **do**  
     $\mathcal{M}_n \leftarrow \{i : x^i = \mathbf{M}\}$   
    **if**  $\mathcal{M}_n = \emptyset$  **then**  
        **break**  
    **end if**  
    Compute logits  $\ell \leftarrow f_\theta(\mathbf{x})$   
    Compute probabilities  $\pi^i \leftarrow \text{softmax}(\ell^i)$  for  $i \in \mathcal{M}_n$   
    Compute confidence  $r^i \leftarrow p_1^i / (p_2^i + \epsilon)$   
    **for**  $i \in \mathcal{M}_n$  **do**  
        Compute  $\phi^i$  via Equation (6)  
         $\tau^i \leftarrow \tau_{\max} - (\tau_{\max} - \tau_{\min}) \cdot \phi^i$   
        **if**  $r^i \geq \tau^i$  **then**  
             $x^i \leftarrow \arg \max_v \pi_v^i$  {Finalize position}  
        **end if**  
    **end for**  
    Apply transfer schedule to remaining masked positions  
  **end for**  
  **return**  $\mathbf{x}$

---

## 4.6 Discussion

**Computational overhead.** The spatial weight computation in Equation (5) can be implemented efficiently via a 1D convolution with a precomputed kernel, adding negligible overhead per step. The dominant cost remains the forward pass through  $f_\theta$ , which JOT reduces by terminating early when all positions are finalized.

**Interaction with transfer schedules.** JOT operates alongside the standard transfer schedule rather than replacing it. At each step, positions that do not meet the early-exit criterion remain masked and are subject to the model’s default unmasking schedule: the transfer schedule determines how many of these remaining positions to reveal based on model predictions. If no positions satisfy the confidence threshold, the step proceeds exactly as in standard decoding. This ensures that the method gracefully degrades to baseline behavior when predictions remain uncertain.

**Orthogonality with other acceleration methods.** JOT is orthogonal to techniques that reduce per-step latency, such as KV-caching methods like dKV-Cache [14] and Fast-dLLM [23]. While these methods accelerate individual forward passes by caching intermediate representations, JOT reduces the total number of steps by early-exiting tokens that have stabilized. The two approaches target different sources of inefficiency and can be combined for compounding speedups: caching reduces per-step cost while JOT reduces step count. We leave the empirical evaluation of such integrated systems as a promising direction for future work.

## 5 Experiments

We evaluate JOT on a diverse set of benchmarks spanning reasoning, knowledge, and code generation. Our experiments aim to answer: (1) Does JOT achieve better speed-quality trade-offs than existing early-stopping methods? (2) How do threshold selection and spatial modulation contribute to performance?

### 5.1 Experimental Setup

We evaluate on two state-of-the-art open diffusion language models: Dream-7B-Instruct [24] and LLaDA-8B-Instruct [15]. We consider four benchmarks: GSM8K [4] for mathematical reasoning with chain-of-thought prompting, MMLU [8] for multitask language understanding, HellaSwag [25] for commonsense reasoning, and HumanEval [3] for code generation. All experiments use zero-shot prompting. Configuration details are summarized in Table 2.

We compare against full decoding (standard diffusion sampling), Prophet [11] (early-commit with top-2 confidence gaps), and KLASS [10] (KL-adaptive stability sampling). We report task-specific scores and *speedup*, defined as

Table 1: Comparison of early-stopping methods on Dream-7B-Instruct and LLaDA-8B-Instruct across four benchmarks. We report task score (%) with gain relative to full decoding, and speedup ( $\times$ ). JOT uses  $\tau_{\max} = 90$ ,  $\tau_{\min} = 1$ ,  $\gamma = 0.5$ ,  $D = 8$  for Dream and  $\tau_{\max} = 30$ ,  $\tau_{\min} = 1$ ,  $\gamma = 0.5$ ,  $D = 8$  for LLaDA.

Model	Method	GSM8K		MMLU		HellaSwag		HumanEval	
		SCORE $\uparrow$	SPEED $\uparrow$	SCORE $\uparrow$	SPEED $\uparrow$	SCORE $\uparrow$	SPEED $\uparrow$	PASS@1 $\uparrow$	SPEED $\uparrow$
DREAM-7B	FULL DECODING	81.1	1.00 $\times$	68.2	1.00 $\times$	73.3	1.00 $\times$	59.1	1.00 $\times$
	PROPHET	68.6 (-12.5)	2.79 $\times$	60.2 (-8.0)	1.40 $\times$	72.4 (-0.9)	1.94 $\times$	56.7 (-2.4)	9.17 $\times$
	KLASS	82.7 (+1.6)	2.45 $\times$	64.4 (-3.8)	1.06 $\times$	74.8 (+1.5)	1.13 $\times$	59.8 (+0.7)	7.92 $\times$
	JOT (OURS)	78.8 (-2.3)	5.54 $\times$	66.7 (-1.5)	1.57 $\times$	72.7 (-0.6)	2.26 $\times$	58.5 (-0.6)	19.60 $\times$
LLADA-8B	FULL DECODING	74.5	1.00 $\times$	67.3	1.00 $\times$	76.7	1.00 $\times$	47.6	1.00 $\times$
	PROPHET	64.4 (-10.1)	2.74 $\times$	63.3 (-4.0)	2.08 $\times$	75.8 (-0.9)	1.84 $\times$	40.9 (-6.7)	1.89 $\times$
	KLASS	74.2 (-0.3)	2.58 $\times$	63.4 (-3.9)	1.26 $\times$	77.1 (+0.4)	1.48 $\times$	40.2 (-7.4)	2.53 $\times$
	JOT (OURS)	73.4 (-1.1)	3.75 $\times$	64.5 (-2.8)	1.98 $\times$	76.6 (-0.1)	3.42 $\times$	44.5 (-3.1)	2.12 $\times$

the ratio of configured to actual steps. All experiments use LM-Evaluation-Harness [6] for reproducibility. Our implementation is built upon the open-source framework provided by [26], which we extend to incorporate JOT.

Ablation studies (Sections 5.3 to 5.5) are conducted on Dream-7B using a subset of each benchmark. Final results in Table 1 use the full benchmark on both Dream-7B and LLaDA-8B.

For MMLU (3 tokens) and HellaSwag (5 tokens), generation length is shorter than typical window sizes  $D$ . The spatial window effectively spans the entire sequence regardless of  $D$ , so results for  $D = 8$  and  $D = 16$  are identical to  $D = 4$ . We report only  $\gamma$  as the varying parameter for these benchmarks.

## 5.2 Main Results

Table 1 presents our main comparison. On Dream-7B, JOT achieves substantial speedups—5.54 $\times$  on GSM8K and 19.60 $\times$  on HumanEval—while incurring only modest accuracy drops (−2.3 and −0.6 points respectively). Prophet shows larger quality degradation, particularly on GSM8K where it drops 12.5 points, and on MMLU where it drops 8.0 points. KLASS maintains strong accuracy on GSM8K (+1.6) but with lower speedup (2.45 $\times$ ) and shows significant MMLU degradation (−3.8 points). On LLaDA-8B, JOT consistently maintains the smallest accuracy gaps across benchmarks while providing competitive speedups. The per-token approach allows positions that genuinely require further refinement to continue through the diffusion chain, while finalizing confident predictions early. Wallclock time analysis (Section A.1) confirms that computational overhead is negligible, and generation quality metrics (Section A.3) show that fluency is preserved.

Figure 3 visualizes the aggregate speed-quality trade-off across all benchmarks on Dream-7B. JOT occupies a favorable position on the Pareto frontier, achieving 7.2 $\times$  average speedup while retaining 98.3% of baseline quality. In contrast, Prophet sacrifices quality for speed (91.9% retention at 3.8 $\times$ ), while KLASS preserves quality but with more limited acceleration (3.2 $\times$ ). This positions JOT as a compelling choice when both speed and accuracy matter.

Table 2: Evaluation configuration for each model and benchmark.

Model	Benchmark	Steps	Block
DREAM-7B	GSM8K	256	—
	MMLU	3	—
	HELLASWAG	5	—
	HUMAN EVAL	512	—
LLADA-8B	GSM8K	256	32
	MMLU	3	3
	HELLASWAG	5	5
	HUMAN EVAL	512	32

Table 3: Ablation on spatial modulation with  $(\tau_{\max}, \tau_{\min}) = (90, 1)$ . Gains are relative to threshold-only baseline ( $\tau = 90$ , no spatial). Results on Dream-7B (subset of benchmark).

GSM8K			MMLU			HellaSwag		HumanEval	
$\gamma$	$D$	SCORE↑	SPEED↑	SCORE↑	SPEED↑	SCORE↑	SPEED↑	PASS@1↑	SPEED↑
<i>No spatial</i>		79.4	5.22×	60.6	1.92×	73.8	2.33×	57.3	19.48×
0.9	16	78.5 (-0.9)	5.82× (+0.60)	66.8 (+6.2)	1.60× (-0.32)	73.6 (-0.2)	2.34× (+0.01)	57.3 (+0.0)	21.94× (+2.46)
0.9	8	77.9 (-1.5)	5.71× (+0.49)	66.8 (+6.2)	1.60× (-0.32)	73.6 (-0.2)	2.34× (+0.01)	58.7 (+1.4)	20.82× (+1.34)
0.7	8	79.7 (+0.3)	5.58× (+0.36)	67.0 (+6.4)	1.58× (-0.34)	73.8 (+0.0)	2.34× (+0.01)	57.3 (+0.0)	20.22× (+0.74)
0.5	16	79.7 (+0.3)	5.49× (+0.27)	66.8 (+6.2)	1.57× (-0.35)	73.6 (-0.2)	2.34× (+0.01)	58.7 (+1.4)	20.03× (+0.55)
0.5	8	80.0 (+0.6)	5.49× (+0.27)	66.8 (+6.2)	1.57× (-0.35)	73.6 (-0.2)	2.34× (+0.01)	58.7 (+1.4)	19.97× (+0.49)
0.5	4	79.4 (+0.0)	5.45× (+0.23)	66.8 (+6.2)	1.57× (-0.35)	73.6 (-0.2)	2.34× (+0.01)	58.0 (+0.7)	19.97× (+0.49)
0.3	8	79.7 (+0.3)	5.45× (+0.23)	66.9 (+6.3)	1.54× (-0.38)	73.6 (-0.2)	2.34× (+0.01)	59.3 (+2.0)	19.90× (+0.42)

Table 4: Hyperparameter sweep on Dream-7B-Instruct. Score (%) with gain relative to full decoding, and speedup (×). Results on subset of benchmark.

GSM8K			MMLU			HellaSwag		HumanEval		
$\tau_{\max}$	$\gamma$	$D$	SCORE↑	SPEED↑	SCORE↑	SPEED↑	SCORE↑	SPEED↑	PASS@1↑	SPEED↑
<i>Full Decoding</i>			82.0	1.00×	68.2	1.00×	73.3	1.00×	59.1	1.00×
60	0.3	8	77.9 (-4.1)	6.12×	67.2 (-1.0)	1.66×	73.6 (+0.3)	2.36×	54.0 (-5.1)	22.81×
60	0.5	8	78.2 (-3.8)	6.19×	67.2 (-1.0)	1.68×	73.5 (+0.2)	2.36×	56.0 (-3.1)	22.74×
60	0.5	16	77.9 (-4.1)	6.19×	67.2 (-1.0)	1.68×	73.5 (+0.2)	2.36×	56.7 (-2.4)	22.70×
60	0.7	8	77.3 (-4.7)	6.29×	67.0 (-1.2)	1.73×	73.6 (+0.3)	2.36×	56.7 (-2.4)	23.07×
90	0.3	8	79.7 (-2.3)	5.45×	66.9 (-1.3)	1.54×	73.6 (+0.3)	2.34×	59.3 (+0.2)	19.90×
90	0.5	8	80.0 (-2.0)	5.49×	66.8 (-1.4)	1.57×	73.6 (+0.3)	2.34×	58.7 (-0.4)	19.97×
90	0.5	16	79.7 (-2.3)	5.49×	66.8 (-1.4)	1.57×	73.6 (+0.3)	2.34×	58.7 (-0.4)	20.03×
90	0.7	8	79.7 (-2.3)	5.58×	67.0 (-1.2)	1.58×	73.8 (+0.5)	2.34×	57.3 (-1.8)	20.22×
120	0.3	8	80.3 (-1.7)	5.13×	66.8 (-1.4)	1.50×	73.7 (+0.4)	2.32×	58.0 (-1.1)	18.04×
120	0.5	8	80.6 (-1.4)	5.16×	67.1 (-1.1)	1.51×	73.6 (+0.3)	2.32×	57.3 (-1.8)	18.25×
120	0.5	16	80.3 (-1.7)	5.16×	67.1 (-1.1)	1.51×	73.6 (+0.3)	2.32×	58.0 (-1.1)	18.22×
120	0.7	8	81.2 (-0.8)	5.23×	67.0 (-1.2)	1.53×	73.6 (+0.3)	2.33×	59.3 (+0.2)	18.75×

### 5.3 Threshold Ablation

We first analyze the effect of the confidence threshold  $\tau$  without spatial modulation (i.e.,  $\tau^i = \tau$  for all positions). This isolates the impact of threshold selection on the speed-quality trade-off.

Table 5 reveals that threshold selection critically affects both quality and speedup. Lower thresholds ( $\tau \leq 30$ ) yield aggressive speedups but cause substantial accuracy drops on reasoning tasks—GSM8K degrades by up to 17.8 points at  $\tau = 10$  and MMLU by 8.8 points. The threshold  $\tau = 90$  provides a favorable balance, achieving 5.22× speedup on GSM8K with only -2.6 points accuracy drop and 19.48× on HumanEval with -1.8 points. Higher thresholds ( $\tau = 120$ ) can exceed baseline quality on some benchmarks (GSM8K +1.9, HumanEval +0.9), though with diminishing speedup returns. Based on these results, we select  $\tau_{\max} = 90$  as the baseline threshold for spatial modulation experiments.

### 5.4 Spatial Modulation Ablation

Having identified  $\tau_{\max} = 90$  as an effective threshold, we now evaluate spatial modulation with  $\tau_{\min} = 1$  (ablation on  $\tau_{\min}$  is provided in Section A.2). We vary the decay rate  $\gamma \in \{0.3, 0.5, 0.7, 0.9\}$  and window size  $D \in \{4, 8, 16\}$ .

Table 3 shows the effect of spatial modulation across decay rates and window sizes. For long-generation benchmarks, spatial modulation provides meaningful speedup gains: HumanEval improves from 19.48× to 21.94× with  $(\gamma, D) = (0.9, 16)$ . The configuration  $(\gamma, D) = (0.5, 8)$  achieves a favorable balance with GSM8K accuracy of 80.0% (+0.6 vs. no spatial) and HumanEval at 58.7% (+1.4). Larger decay rates ( $\gamma = 0.9$ ) spread influence too broadly, causing accuracy degradation on GSM8K (-1.5 points at  $\gamma = 0.9, D = 8$ ). Based on these findings, we select  $(\gamma, D) = (0.5, 8)$  as the default spatial configuration.

Table 5: Ablation on confidence threshold without spatial modulation. We report score (%) with gain relative to full decoding, and speedup ( $\times$ ). Results on Dream-7B (subset of benchmark).

$\tau$	GSM8K		MMLU		HellaSwag		HumanEval	
	SCORE $\uparrow$	SPEED $\uparrow$	SCORE $\uparrow$	SPEED $\uparrow$	SCORE $\uparrow$	SPEED $\uparrow$	PASS@1 $\uparrow$	SPEED $\uparrow$
<i>Full Decoding</i>	82.0	1.00 $\times$	68.2	1.00 $\times$	73.3	1.00 $\times$	59.1	1.00 $\times$
10	64.2 (-17.8)	11.10 $\times$	59.4 (-8.8)	2.44 $\times$	73.6 (+0.3)	2.44 $\times$	42.7 (-16.4)	43.21 $\times$
30	77.0 (-5.0)	7.12 $\times$	59.6 (-8.6)	2.19 $\times$	73.6 (+0.3)	2.38 $\times$	53.3 (-5.8)	28.65 $\times$
60	75.8 (-6.2)	5.92 $\times$	60.5 (-7.7)	2.02 $\times$	73.5 (+0.2)	2.36 $\times$	57.3 (-1.8)	21.82 $\times$
90	79.4 (-2.6)	5.22 $\times$	60.6 (-7.6)	1.92 $\times$	73.8 (+0.5)	2.33 $\times$	57.3 (-1.8)	19.48 $\times$
120	83.9 (+1.9)	4.90 $\times$	60.7 (-7.5)	1.86 $\times$	74.0 (+0.7)	2.31 $\times$	60.0 (+0.9)	17.64 $\times$
150	82.7 (+0.7)	4.64 $\times$	60.5 (-7.7)	1.80 $\times$	73.6 (+0.3)	2.25 $\times$	56.7 (-2.4)	16.79 $\times$

Table 6: Threshold ablation on LLaDA-8B-Instruct (subset of each benchmark). Spatial modulation uses  $\gamma = 0.5$ ,  $D = 8$ . Score gain is relative to full decoding baseline.

$\tau_{\max}$	GSM8K		MMLU		HellaSwag		HumanEval	
	SCORE $\uparrow$	SPEED $\uparrow$	SCORE $\uparrow$	SPEED $\uparrow$	SCORE $\uparrow$	SPEED $\uparrow$	PASS@1 $\uparrow$	SPEED $\uparrow$
BASELINE	74.5	1.00 $\times$	67.3	1.00 $\times$	76.7	1.00 $\times$	47.6	1.00 $\times$
10	32.2 (-42.3)	8.97 $\times$	63.8 (-3.5)	2.21 $\times$	72.7 (-4.0)	4.16 $\times$	41.4 (-6.2)	3.50 $\times$
30	72.1 (-2.4)	3.54 $\times$	63.8 (-3.5)	1.98 $\times$	72.7 (-4.0)	3.27 $\times$	45.1 (-2.5)	2.12 $\times$
60	75.8 (+1.3)	2.69 $\times$	63.8 (-3.5)	1.85 $\times$	72.7 (-4.0)	2.03 $\times$	45.5 (-2.1)	1.77 $\times$
90	79.8 (+5.3)	2.45 $\times$	63.8 (-3.5)	1.77 $\times$	72.7 (-4.0)	1.64 $\times$	44.5 (-3.1)	1.62 $\times$
120	79.1 (+4.6)	2.36 $\times$	63.8 (-3.5)	1.71 $\times$	72.7 (-4.0)	1.33 $\times$	44.1 (-3.5)	1.51 $\times$
150	78.2 (+3.7)	2.24 $\times$	63.8 (-3.5)	1.65 $\times$	72.7 (-4.0)	1.21 $\times$	43.9 (-3.7)	1.44 $\times$

## 5.5 Hyperparameter Sweep

Finally, we conduct a sweep around the identified optimal parameters:

$\tau_{\max} \in \{60, 90, 120\}$  and  $(\gamma, D) \in \{(0.3, 4), (0.3, 8), (0.5, 4), (0.5, 8)\}$ , with  $\tau_{\min} = 1$  fixed.

Table 4 confirms that JOT maintains robust performance across a range of hyperparameter configurations. Lower thresholds ( $\tau_{\max} = 60$ ) trade more accuracy for speed, while higher thresholds ( $\tau_{\max} = 120$ ) often exceed baseline quality with more modest speedups. The configuration  $(\tau_{\max}, \gamma, D) = (90, 0.5, 8)$  provides a balanced default, but practitioners can adjust based on their accuracy-speed priorities. This stability reduces the need for extensive task-specific tuning, making the method practical for deployment across diverse applications.

## 5.6 LLaDA Threshold Ablation

To verify generalization across model architectures, we conduct a threshold ablation on LLaDA-8B (Table 6). LLaDA exhibits different sensitivity patterns than Dream: GSM8K benefits from higher thresholds ( $\tau = 60$ –90 achieve accuracy above baseline), while MMLU and HellaSwag show consistent scores across all thresholds with varying speedups. Based on these results, we select  $\tau_{\max} = 30$  for LLaDA in the main comparison, as it provides strong speedups (3.54 $\times$  on GSM8K, 1.98 $\times$  on MMLU) while maintaining close to baseline quality on reasoning tasks.

## 5.7 Confidence Dynamics

To understand how JOT affects the generation process, we visualize the mean confidence ratio across diffusion steps for two randomly selected GSM8K samples (Figures 1 and 2).

The baseline decoding exhibits a characteristic pattern: confidence starts very high and declines smoothly over steps. This occurs because the standard transfer schedule forces the model to unmask tokens gradually, even when many positions are already highly confident. The model effectively spends early steps filling in “obvious” context tokens that it could predict immediately, before entering a lower-confidence reasoning phase where it works on the actual answer.

JOT fundamentally changes this dynamic. By allowing early exit for confident predictions, the method permits the model to finalize obvious tokens instantly and proceed directly to the reasoning phase. This manifests as a rapid

### Q1088: A farmer is baling hay in their field

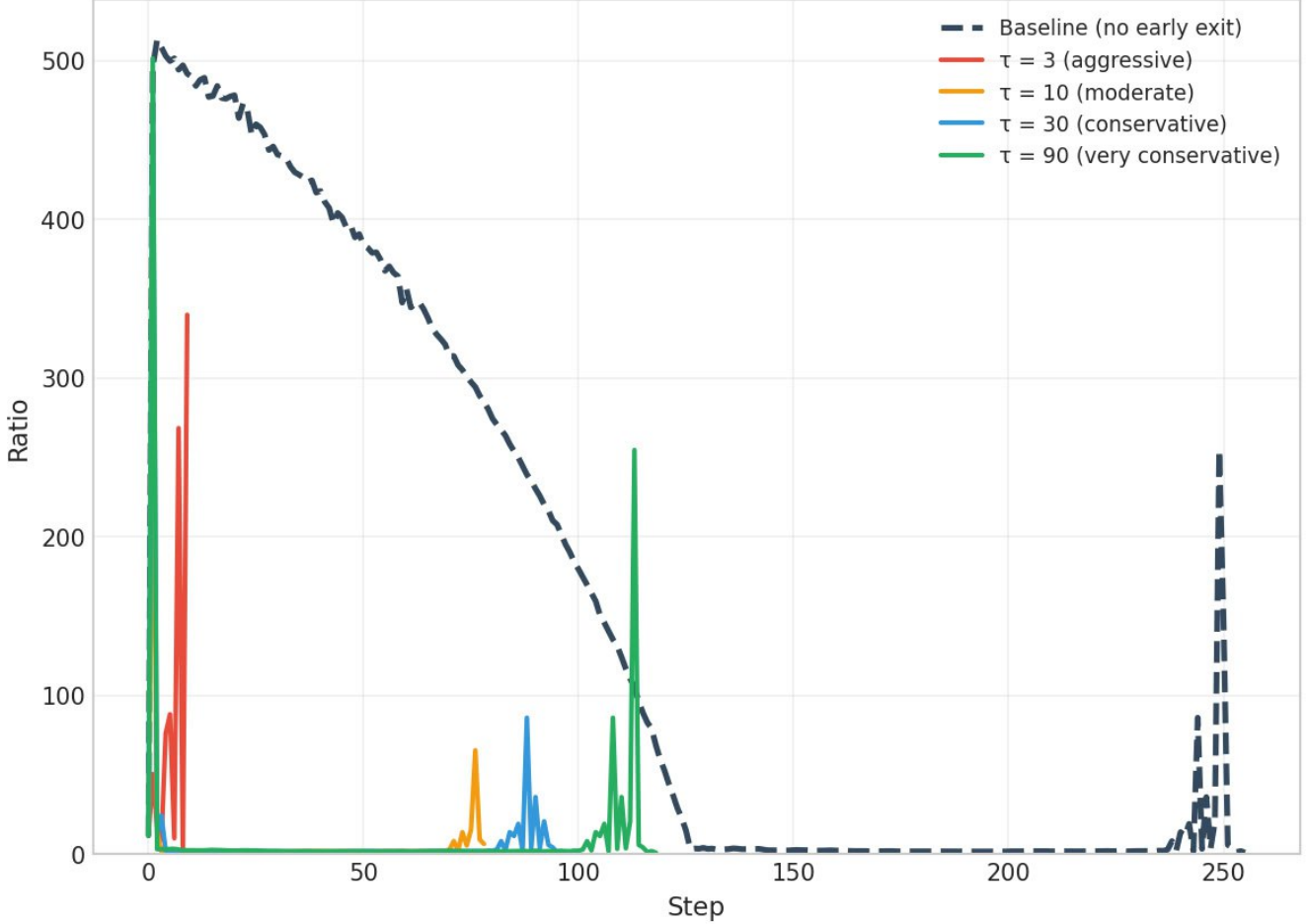


Figure 1: Confidence ratio dynamics for a GSM8K sample. The baseline (dashed) shows a smooth decline as the sampler gradually unmasks tokens. JOT with  $\tau = 90$  rapidly finalizes high-confidence tokens, then exhibits spikes during the reasoning phase before converging to a similar pattern as the baseline.

initial drop in mean confidence (as high-confidence positions exit), followed by sustained activity during reasoning. Crucially, with conservative thresholds ( $\tau = 90$ ), the confidence pattern at the end of the reasoning phase closely mirrors that of the baseline, indicating that the model follows a similar computational trajectory to arrive at the answer.

Aggressive thresholds ( $\tau = 3$ ) exit too early, cutting off the reasoning process before the model can fully work through the problem. This explains the accuracy degradation observed in Table 5. More conservative thresholds ( $\tau = 30, 60$ ) provide sufficient time for reasoning while still achieving substantial speedups by eliminating redundant refinement of already-converged positions.

## Q167: Sandra's neighbor gives her a basket of 9...

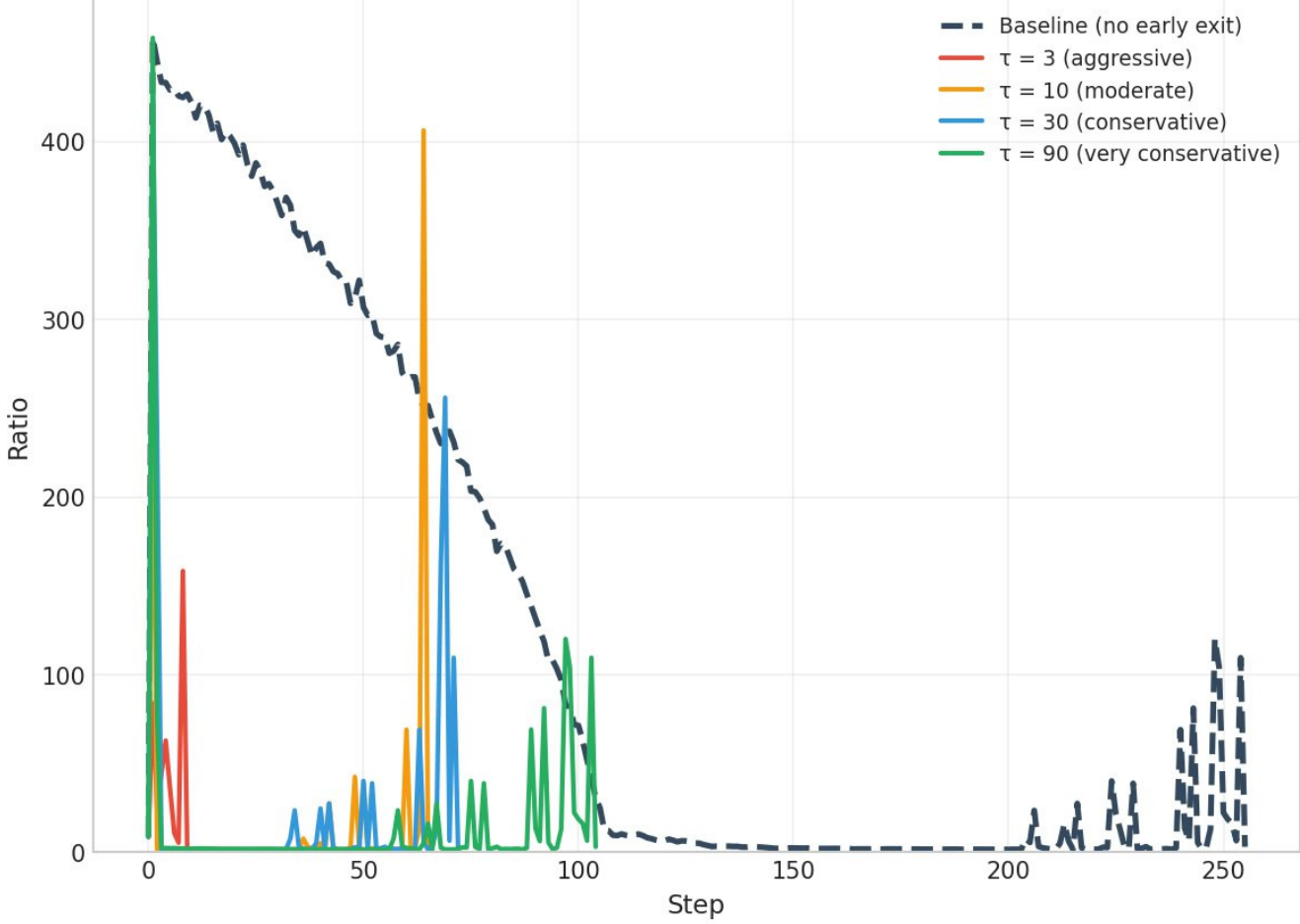


Figure 2: Confidence ratio dynamics for another GSM8K sample. Conservative thresholds ( $\tau \geq 30$ ) allow the model to reach the reasoning phase and produce answer patterns similar to the baseline, while aggressive thresholds ( $\tau = 3$ ) exit prematurely.

## 6 Limitations

While JOT demonstrates favorable speed-quality trade-offs on the benchmarks studied, several limitations warrant discussion.

Early stopping at the token level may affect text fluency or coherence in ways task-specific metrics do not capture. Our preliminary analysis on open-ended generation (Section A.3) shows that JOT maintains comparable perplexity and reduces repetition, though MAUVE scores are moderately lower. Comprehensive evaluation across diverse generation tasks and human judgment studies remains for future work.

JOT finalizes tokens using argmax selection once the confidence threshold is exceeded. This greedy approach foregoes alternative token choices that might yield better global solutions. How to integrate JOT with sampling-based decoding strategies remains an open question.

Although our hyperparameter sweep shows reasonable robustness, optimal thresholds may still vary across tasks and domains. Our experiments focus on instruction-following benchmarks. Other domains such as creative writing or translation may require different configurations.

Experiments cap generation at 256–512 tokens (Table 2). Behavior on longer sequences (e.g., 1024 or 2048 tokens) is unexplored. Spatial modulation effects may compound differently at scale, and the cumulative impact of many early-exit decisions on coherence is unknown.

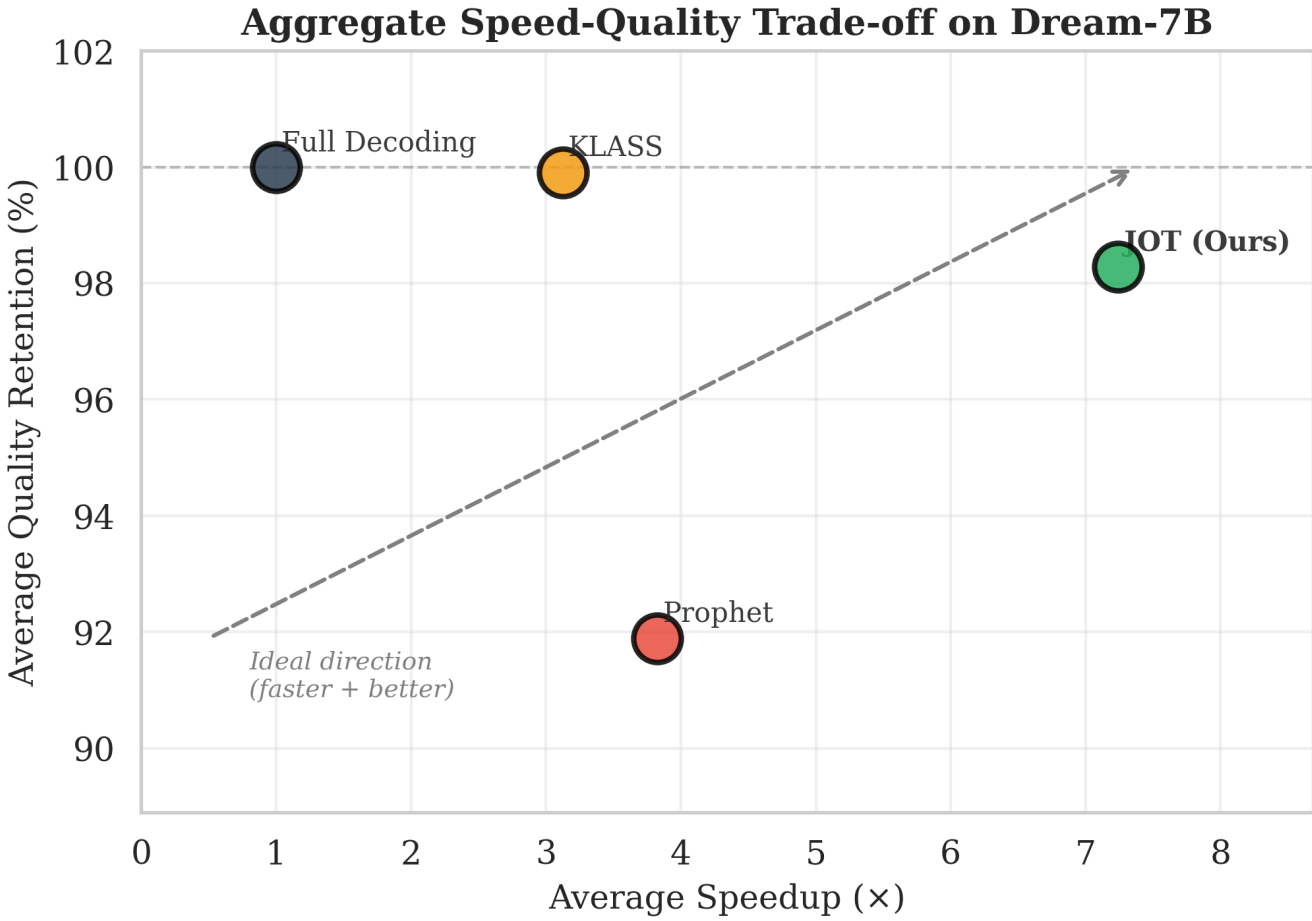


Figure 3: Aggregate speed-quality trade-off on Dream-7B, averaged across all benchmarks. JOT achieves the best Pareto positioning: 7.2 $\times$  average speedup while retaining 98.3% of baseline quality.

## 7 Conclusion

We presented JOT, a training-free method for per-token early stopping in diffusion language models. By monitoring prediction confidence at each position independently and applying spatially-adaptive thresholds, JOT allows different tokens to exit at different steps, concentrating computation on positions that genuinely require further refinement. Experiments on Dream-7B and LLaDA-8B across diverse benchmarks demonstrate that JOT achieves substantial speedups while maintaining competitive accuracy, consistently outperforming existing early-stopping methods in speed-quality trade-offs.

We release our implementation and experimental code at [1].

## References

- [1] Anonymous. jot. <https://github.com/Anonym-cybersudo/JoT>, 2026.
- [2] Jacob Austin, Daniel D. Johnson, Jonathan Ho, Daniel Tarlow, and Rianne van den Berg. Structured denoising diffusion models in discrete state-spaces, 2023. URL <https://arxiv.org/abs/2107.03006>.
- [3] Mark Chen, Jerry Tworek, Heewoo Jun, Qiming Yuan, Henrique Ponde de Oliveira Pinto, Jared Kaplan, Harri Edwards, Yuri Burda, Nicholas Joseph, Greg Brockman, Alex Ray, Raul Puri, Gretchen Krueger, Michael Petrov, Heidy Khlaaf, Girish Sastry, Pamela Mishkin, Brooke Chan, Scott Gray, Nick Ryder, Mikhail Pavlov, Alethea Power, Lukasz Kaiser, Mohammad Bavarian, Clemens Winter, Philippe Tillet, Felipe Petroski Such, Dave Cummings, Matthias Plappert, Fotios Chantzis, Elizabeth Barnes, Ariel Herbert-Voss, William Heben Guss, Alex Nichol, Alex Paino, Nikolas Tezak, Jie Tang, Igor Babuschkin, Suchir Balaji, Shantanu Jain, William Saunders, Christopher Hesse, Andrew N. Carr, Jan Leike, Josh Achiam, Vedant Misra, Evan Morikawa, Alec Radford, Matthew Knight, Miles Brundage, Mira Murati, Katie Mayer, Peter Welinder, Bob McGrew, Dario Amodei, Sam McCandlish, Ilya Sutskever, and Wojciech Zaremba. Evaluating large language models trained on code. 2021.
- [4] Karl Cobbe, Vineet Kosaraju, Mohammad Bavarian, Mark Chen, Heewoo Jun, Lukasz Kaiser, Matthias Plappert, Jerry Tworek, Jacob Hilton, Reiichiro Nakano, Christopher Hesse, and John Schulman. Training verifiers to solve math word problems. *arXiv preprint arXiv:2110.14168*, 2021.
- [5] Jacob Devlin, Ming-Wei Chang, Kenton Lee, and Kristina Toutanova. Bert: Pre-training of deep bidirectional transformers for language understanding, 2019. URL <https://arxiv.org/abs/1810.04805>.
- [6] Leo Gao, Jonathan Tow, Baber Abbasi, Stella Biderman, Sid Black, Anthony DiPofi, Charles Foster, Laurence Golding, Jeffrey Hsu, Alain Le Noac'h, Haonan Li, Kyle McDonell, Niklas Muennighoff, Chris Ociepa, Jason Phang, Laria Reynolds, Hailey Schoelkopf, Aviya Skowron, Lintang Sutawika, Eric Tang, Anish Thite, Ben Wang, Kevin Wang, and Andy Zou. The language model evaluation harness, 07 2024. URL <https://zenodo.org/records/12608602>.
- [7] Shansan Gong, Mukai Li, Jiangtao Feng, Zhiyong Wu, and Lingpeng Kong. Diffuseq: Sequence to sequence text generation with diffusion models, 2023. URL <https://arxiv.org/abs/2210.08933>.
- [8] Dan Hendrycks, Collin Burns, Steven Basart, Andy Zou, Mantas Mazeika, Dawn Song, and Jacob Steinhardt. Measuring massive multitask language understanding, 2021. URL <https://arxiv.org/abs/2009.03300>.
- [9] Jonathan Ho, Ajay Jain, and Pieter Abbeel. Denoising diffusion probabilistic models, 2020. URL <https://arxiv.org/abs/2006.11239>.
- [10] Seo Hyun Kim, Sunwoo Hong, Hojung Jung, Youngrok Park, and Se-Young Yun. Klass: Kl-guided fast inference in masked diffusion models, 2025. URL <https://arxiv.org/abs/2511.05664>.
- [11] Pengxiang Li, Yefan Zhou, Dilxat Muhtar, Lu Yin, Shilin Yan, Li Shen, Yi Liang, Soroush Vosoughi, and Shiwei Liu. Diffusion language models know the answer before decoding, 2025. URL <https://arxiv.org/abs/2508.19982>.
- [12] Xiang Lisa Li, John Thickstun, Ishaan Gulrajani, Percy Liang, and Tatsunori B. Hashimoto. Diffusion-lm improves controllable text generation, 2022. URL <https://arxiv.org/abs/2205.14217>.
- [13] Aaron Lou, Chenlin Meng, and Stefano Ermon. Discrete diffusion modeling by estimating the ratios of the data distribution, 2024. URL <https://arxiv.org/abs/2310.16834>.
- [14] Xinyin Ma, Runpeng Yu, Gongfan Fang, and Xinchao Wang. dkv-cache: The cache for diffusion language models, 2025. URL <https://arxiv.org/abs/2505.15781>.
- [15] Shen Nie, Fengqi Zhu, Zebin You, Xiaolu Zhang, Jingyang Ou, Jun Hu, Jun Zhou, Yankai Lin, Ji-Rong Wen, and Chongxuan Li. Large language diffusion models, 2025. URL <https://arxiv.org/abs/2502.09992>.
- [16] Krishna Pillutla, Swabha Swayamdipta, Rowan Zellers, John Thickstun, Sean Welleck, Yejin Choi, and Zaid Harchaoui. Mauve: Measuring the gap between neural text and human text using divergence frontiers, 2021. URL <https://arxiv.org/abs/2102.01454>.

- [17] Alec Radford, Jeffrey Wu, Rewon Child, David Luan, Dario Amodei, Ilya Sutskever, et al. Language models are unsupervised multitask learners. *OpenAI blog*, 1(8):9, 2019.
- [18] Colin Raffel, Noam Shazeer, Adam Roberts, Katherine Lee, Sharan Narang, Michael Matena, Yanqi Zhou, Wei Li, and Peter J. Liu. Exploring the limits of transfer learning with a unified text-to-text transformer, 2023. URL <https://arxiv.org/abs/1910.10683>.
- [19] Subham Sekhar Sahoo, Marianne Arriola, Yair Schiff, Aaron Gokaslan, Edgar Marroquin, Justin T Chiu, Alexander Rush, and Volodymyr Kuleshov. Simple and effective masked diffusion language models, 2024. URL <https://arxiv.org/abs/2406.07524>.
- [20] Yang Song, Jascha Sohl-Dickstein, Diederik P. Kingma, Abhishek Kumar, Stefano Ermon, and Ben Poole. Score-based generative modeling through stochastic differential equations, 2021. URL <https://arxiv.org/abs/2011.13456>.
- [21] Xu Wang, Chenkai Xu, Yijie Jin, Jiachun Jin, Hao Zhang, and Zhijie Deng. Diffusion llms can do faster-than-ar inference via discrete diffusion forcing, 2025. URL <https://arxiv.org/abs/2508.09192>.
- [22] Qingyan Wei, Yaojie Zhang, Zhiyuan Liu, Dongrui Liu, and Linfeng Zhang. Accelerating diffusion large language models with slowfast sampling: The three golden principles, 2025. URL <https://arxiv.org/abs/2506.10848>.
- [23] Chengyue Wu, Hao Zhang, Shuchen Xue, Zhijian Liu, Shizhe Diao, Ligeng Zhu, Ping Luo, Song Han, and Enze Xie. Fast-dllm: Training-free acceleration of diffusion llm by enabling kv cache and parallel decoding, 2025. URL <https://arxiv.org/abs/2505.22618>.
- [24] Jiacheng Ye, Zhihui Xie, Lin Zheng, Jiahui Gao, Zirui Wu, Xin Jiang, Zhenguo Li, and Lingpeng Kong. Dream 7b: Diffusion large language models, 2025. URL <https://arxiv.org/abs/2508.15487>.
- [25] Rowan Zellers, Ari Holtzman, Yonatan Bisk, Ali Farhadi, and Yejin Choi. Hellaswag: Can a machine really finish your sentence?, 2019. URL <https://arxiv.org/abs/1905.07830>.
- [26] Zhanhui Zhou, Lingjie Chen, Hanghang Tong, and Dawn Song. dllm: Simple diffusion language modeling. <https://github.com/ZHZisZZ/dllm>, 2025.

## A Additional Experiments

### A.1 Wallclock Time Analysis

The step-based speedup reported in the main text measures the reduction in diffusion steps, which directly correlates with the number of forward passes through the model. However, practical deployment also involves per-step overhead from confidence computation and early-exit bookkeeping. Table 7 reports wallclock speedups measured on a single NVIDIA A100 GPU.

Table 7: Wallclock time comparison on Dream-7B-Instruct and LLaDA-8B-Instruct. We report task score (%) with gain relative to full decoding, and wallclock speedup ( $\times$ ).

Model	Method	GSM8K		MMLU		HellaSwag		HumanEval	
		SCORE↑	SPEED↑	SCORE↑	SPEED↑	SCORE↑	SPEED↑	PASS@1↑	SPEED↑
DREAM-7B	FULL DECODING	81.1	1.00 $\times$	68.2	1.00 $\times$	73.3	1.00 $\times$	59.1	1.00 $\times$
	PROPHET	68.6 (-12.5)	2.41 $\times$	60.2 (-8.0)	1.38 $\times$	72.4 (-0.9)	1.91 $\times$	56.7 (-2.4)	6.82 $\times$
	KLASS	82.7 (+1.6)	2.12 $\times$	64.4 (-3.8)	1.08 $\times$	74.8 (+1.5)	1.05 $\times$	59.8 (+0.7)	5.94 $\times$
	JOT (OURS)	78.8 (-2.3)	4.21 $\times$	66.7 (-1.5)	1.54 $\times$	72.7 (-0.6)	2.22 $\times$	58.5 (-0.6)	12.35 $\times$
LLADA-8B	FULL DECODING	74.5	1.00 $\times$	67.3	1.00 $\times$	76.7	1.00 $\times$	47.6	1.00 $\times$
	PROPHET	64.4 (-10.1)	2.38 $\times$	63.3 (-4.0)	2.04 $\times$	75.8 (-0.9)	1.81 $\times$	40.9 (-6.7)	1.72 $\times$
	KLASS	74.2 (-0.3)	1.92 $\times$	63.4 (-3.9)	1.24 $\times$	77.1 (+0.4)	1.41 $\times$	40.2 (-7.4)	2.18 $\times$
	JOT (OURS)	73.4 (-1.1)	3.07 $\times$	64.5 (-2.8)	1.61 $\times$	76.6 (-0.1)	2.88 $\times$	44.5 (-3.1)	1.94 $\times$

For long-generation tasks (GSM8K, HumanEval), the overhead is amortized over many steps, and wallclock speedups remain substantial: JOT achieves 4.21 $\times$  on GSM8K and 12.35 $\times$  on HumanEval for Dream-7B. For short-generation tasks (MMLU, HellaSwag), the overhead represents a larger fraction of total time, resulting in wallclock speedups closer to step-based speedups. Overall, the computational overhead of JOT is negligible relative to the savings from reduced forward passes.

### A.2 Effect of Minimum Threshold

The spatial modulation mechanism interpolates thresholds between  $\tau_{\max}$  and  $\tau_{\min}$  based on proximity to unmasked tokens. We investigate whether the choice of  $\tau_{\min}$  significantly affects performance by comparing  $\tau_{\min} = 1$  (used in main experiments) with  $\tau_{\min} = 30$ .

Table 8: Comparison of  $\tau_{\min} = 1$  vs.  $\tau_{\min} = 30$  with  $\tau_{\max} = 90$ . Higher  $\tau_{\min}$  provides no meaningful benefit. Results on Dream-7B (subset of benchmark).

$\gamma$	$D$	GSM8K				HumanEval			
		$\tau_{\min} = 1$		$\tau_{\min} = 30$		$\tau_{\min} = 1$		$\tau_{\min} = 30$	
		SCORE	SPEED	SCORE	SPEED	PASS@1	SPEED	PASS@1	SPEED
0.9	16	78.5	5.82 $\times$	78.0	5.51 $\times$	57.3	21.94 $\times$	58.0	19.63 $\times$
0.9	8	77.9	5.71 $\times$	78.0	5.38 $\times$	58.7	20.82 $\times$	57.3	19.78 $\times$
0.7	8	79.7	5.58 $\times$	77.3	5.34 $\times$	57.3	20.22 $\times$	58.7	19.71 $\times$
0.5	16	79.7	5.49 $\times$	77.3	5.31 $\times$	58.7	20.03 $\times$	57.3	19.73 $\times$
0.5	8	80.0	5.49 $\times$	77.3	5.30 $\times$	58.7	19.97 $\times$	58.7	19.70 $\times$
0.5	4	79.4	5.45 $\times$	78.0	5.28 $\times$	58.0	19.97 $\times$	58.0	19.85 $\times$
0.3	8	79.7	5.45 $\times$	77.3	5.27 $\times$	59.3	19.90 $\times$	58.7	19.61 $\times$

Table 8 shows that increasing  $\tau_{\min}$  from 1 to 30 provides no meaningful benefit. On GSM8K, accuracy remains within 1-2 points across configurations, while speedups are slightly lower with  $\tau_{\min} = 30$  due to the reduced range of threshold modulation. On HumanEval, both settings achieve similar accuracy (57–59%) with comparable speedups. These results suggest that the primary driver of performance is  $\tau_{\max}$ , and positions benefiting from spatial modulation (those near context boundaries) can safely use very low thresholds without degrading quality. We therefore use  $\tau_{\min} = 1$  as the default setting.

### A.3 Generation Quality Metrics

To assess whether early stopping affects generation fluency beyond task accuracy, we evaluate open-ended text continuation on 512 samples from the C4 dataset [18] with 256 generated tokens using Dream-7B.

Table 9: Generation quality metrics on C4 continuations (256 tokens). Lower is better for Repetition and Perplexity; higher is better for MAUVE.

Method	MAUVE $\uparrow$	Rep-4 $\downarrow$	PPL $\downarrow$
FULL DECODING	0.941	0.216	5.88
JOT ( $\tau = 90$ )	0.831	0.176	5.94

Table 9 reports MAUVE [16] for distributional similarity, 4-gram repetition rate, and perplexity computed by GPT-2 Medium [17]. JOT achieves *lower* repetition (0.176 vs. 0.216), suggesting that early stopping may help avoid degenerate repetitive patterns. Perplexity remains comparable (5.94 vs. 5.88), indicating that fluency is preserved. MAUVE is moderately lower (0.831 vs. 0.941), which may reflect the distributional shift from early-exited tokens; however, both values indicate reasonable alignment with reference text distributions.